Minerals Engineering 217 (2024) 108918

Contents lists available at ScienceDirect

Minerals Engineering

journal homepage: www.elsevier.com/locate/mineng

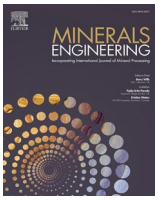

Valorization of lithium containing slags from pyrometallurgical recycling route of spent lithium-ion batteries: The enrichment of γ-$LiAlO_2$ phase from thermodynamic controlled and modified slags

Hao Qiu [a,*], Haojie Li [b], Michael Fischlschweiger [b], Marko Ranneberg [c], Torsten Graupner [c], Hugo Lucas [d], Christin Stallmeister [d], Bernd Friedrich [d], Bengi Yagmurlu [a], Daniel Goldmann [a]

[a] Institute of Mineral and Waste Processing, Recycling and Circular Economy Systems (IFAD), Clausthal University of Technology, Walther-Nernst-Straße 9, 38678 Clausthal-Zellerfeld, Germany
[b] Chair of Technical Thermodynamics and Energy Efficient Material Treatment, Institute of Energy Process Engineering and Fuel Technology (IEVB), Clausthal University of Technology, Agricolastraße 4, 38678 Clausthal-Zellerfeld, Germany
[c] Federal Institute for Geosciences and Natural Resources (BGR), Stilleweg 2, 30655 Hannover, Germany
[d] Institute of Process Metallurgy and Metal Recycling (IME), RWTH Aachen University, Intzestr. 3, 52056 Aachen, Germany

ARTICLE INFO

Keywords:
Engineering of Artificial Minerals
EnAM
Slag flotation
Battery recycling
Slag valorization
Lithium recovery

ABSTRACT

Pyro-metallurgical processing technology is widely used in the spent lithium-ion batteries recycling to recover valuable metals such as cobalt, nickel and copper, while lithium primarily remains in the slag. The effective valorization of slag, especially lithium recovery, constitutes a significant issue in contemporary pyrometallurgical processes due to the paucity of studies. This paper proposes a novel perspective by defining slag as an aggregate of engineered artificial minerals. Thus, not only the parameters of the beneficiation process can be studied to optimize the separation efficiency during treatment, but also the slag can be re-designed to optimize the carrier minerals of target elements and gangue mineral composition in the initial step with thermodynamic tools. In this paper, the engineering of artificial minerals (EnAM) method was applied to the slag design of the Li_2O-CaO-Al_2O_3-SiO_2-MnO system, and an initial attempt was made to apply EnAM method to the flotation study. A flotation study on enrichment effect of the target phase γ-$LiAlO_2$ from thermodynamic controlled slags is conducted.

1. Introduction

High-temperature pyrometallurgy plays a pivotal role in treating diverse End-of-Life (EoL) components, including waste electrical and electronic equipment (WEEE), metal scraps and lithium-ion batteries (LIBs) (Alvear et al., 2016; Alvear et al., 2014; Elwert et al., 2012; Georgi-Maschler et al., 2012; Davenport et al., 2002; Zhang et al., 2016). Various smelting technologies, such as electric arc furnaces, rotary kilns, or ISASMELT, are employed in this crucial step (Alvear et al., 2014; Friedrich et al., 2018; Lucas et al., 2020). These techniques leverage a slag phase to facilitate the coagulation of metals while gangue and impurities are assimilated into the mineral phase (Fathi Habashi, 1997; Krüger, 1999).

There are two main approaches to recycle LIBs via pyrometallurgical processes. The first involves smelting the entire battery cells without any prior treatment. The second approach entails pretreating the cells to mechanically separate some of the metals, such as aluminum, copper, and iron, before smelting the remaining elements, often known as "black mass" (Elwert et al., 2012; Sommerfeld et al., 2020). Typical industrial processes, e.g. the Umicore process aligns with the first approach, metals such as copper, cobalt, and nickel are reduced to an alloy. This metal phase is collected at the bottom of the furnace, while lithium primarily ends up in the slag phase (Elwert et al., 2012; Sommerfeld et al., 2020).

Throughout the smelting process, the precise selection of fluxes is imperative to control the melting point and viscosity, thus ensuring effective phase separation between the metal phase and the slag (Müller and Friedrich, 2006; Vest et al., 2010; Vignes, 2010). For example, the CaO-Al_2O_3-SiO_2 system is employed in numerous pyrometallurgical procedures for EoL LIBs (Cheret and Santén, 2005; Georgi-Maschler et al., 2012; REN et al., 2017). Following cooling, minerals such as silicates and aluminates often appear in the slag, hence, the slag can also be considered as an artificial mineral aggregate (Elwert et al., 2014; Li

* Corresponding author.

https://doi.org/10.1016/j.mineng.2024.108918
Received 22 March 2024; Received in revised form 25 July 2024; Accepted 7 August 2024
Available online 15 August 2024

et al., 2022; Schirmer et al., 2022; Schirmer et al., 2020; Wittkowski et al., 2021). The valorization of slag, notably the efficient extraction of lithium from the slag, has become a pivotal issue in the contemporary pyrometallurgical recycling pathway for LIBs.

Klimko et al. carried out a leaching study on lithium-bearing slags. The results indicate that the leaching efficiency of lithium can approach nearly 100 % at a leaching temperature of 80 °C (Klimko et al., 2020). However, if a lithium-bearing slag is leached directly, a large amount of silica gel can be produced, which will interfere with filtration and further lithium extraction (Klimko et al., 2020). Therefore, the addition of a beneficiation process prior to the hydrometallurgical process is required. Separating of the lithium aluminate phase from silicate phases, on the one hand, reduces the probability of silica gel formation and at the same time reduces the processing volume of the leaching process, which is of great importance for the optimization of the hydrometallurgical part that is combined with pyrometallurgical recycling route of lithium-ion batteries. The chemical use could significantly reduce upon elimination of the untargeted minerals via the application of beneficiation methods. Furthermore, the dispersion of lithium in different mineral phases in the slag can make the beneficiation process difficult, and how to control the degree of lithium dispersion has become a scientific question. To close this knowledge gap, the Engineering of Artificial Minerals (EnAM) strategy has been used to control lithium dispersion.

The EnAM strategy is a method that uses thermodynamic and kinetic tools to design slags. The initial step involves the selection of an appropriate carrier mineral for the target element, coupled with designing the gangue composition of the slag. The purpose is twofold: first, to pre-enrich the target element in the carrier mineral during the smelting process, and second, to facilitate subsequent beneficiation and hydrometallurgical treatment through the designed carrier mineral and gangue composition. A significant advantage of this approach is the ability to select carrier minerals with high loading capacity for the target element, even those that are non-existent or extremely rare in natural ores. Depending on the processing properties of the common slag constituents, a suitable cooling regime can be chosen for the slag mineral crystal size and morphology. Fig. 1 presents the schematic sketch of EnAM method.

Common carrier minerals for lithium in natural hard rock minerals include spodumene, petalite and lepidolite (Garrett, 2004; Meshram et al., 2014). In these minerals, the theoretical maximum lithium content ranges between 2 wt% and 4 wt% (Garrett, 2004; Meshram et al., 2014). Through the EnAM strategy, within the $CaO\text{-}Al_2O_3\text{-}SiO_2$ system, it is possible to select carrier minerals for lithium such as γ-lithium aluminate (γ-$LiAlO_2$), with a theoretical lithium content of up to 10.5 wt %. In our prior fundamental investigations, we conducted thermodynamic and mineralogical research on the oxide system containing lithium (Li et al., 2022; Schirmer et al., 2022; Schirmer et al., 2020; Wittkowski et al., 2021).

In essence, the core of this approach is the development of robust thermodynamic databases and models, as well as a thorough understanding of the processing properties of typical slag minerals, such as floatability and leachability. The thermodynamic databases and models are the fundamental tools to predict the final slag mineral composition and the distribution of the target elements as a result of varying feed compositions. The accuracy of these models and databases directly influences the precision of the final predictions.

From another perspective, conventional slag treatment or beneficiation research (Refer to Fig. 2) is reliant on the nature of the mineral, and the treatment process is established by continuous optimization of treatment parameters such as grinding time or optimizing the reagent regime. In essence, it is a methodology in which the material determines the process. However, an EnAM slag is designed to adapt to a simplified process or an already established treatment process which directly increases the performance of the beneficiation efficiency (Refer to Fig. 3). Viewed from this perspective, the workload of the beneficiation study can be greatly reduced.

The approach of utilizing slag to enrich target elements has already appeared in other material systems, such as those rare earth elements (REE) containing system and Ti containing system (Elwert et al., 2014; Kai Tang et al., 2013; Mingyu et al., 2006; Müller and Friedrich, 2006; Ren et al., 2017; WANG et al., 2006; Zhang et al., 2007; Zhang et al., 2016). Nonetheless, prior research has primarily concentrated on qualitatively elucidating the enrichment correlation between a specific carrier mineral and the target element, or the connection between the composition of feedstock and a mineral phase in the slag, rather than systematically studying it.

This paper is a preliminary attempt to use the EnAM strategy for slag design and slag processing in the $Li_2O\text{-}CaO\text{-}Al_2O_3\text{-}SiO_2\text{-}MnO$ system. A systematic study was conducted on the flotation enrichment effect of the

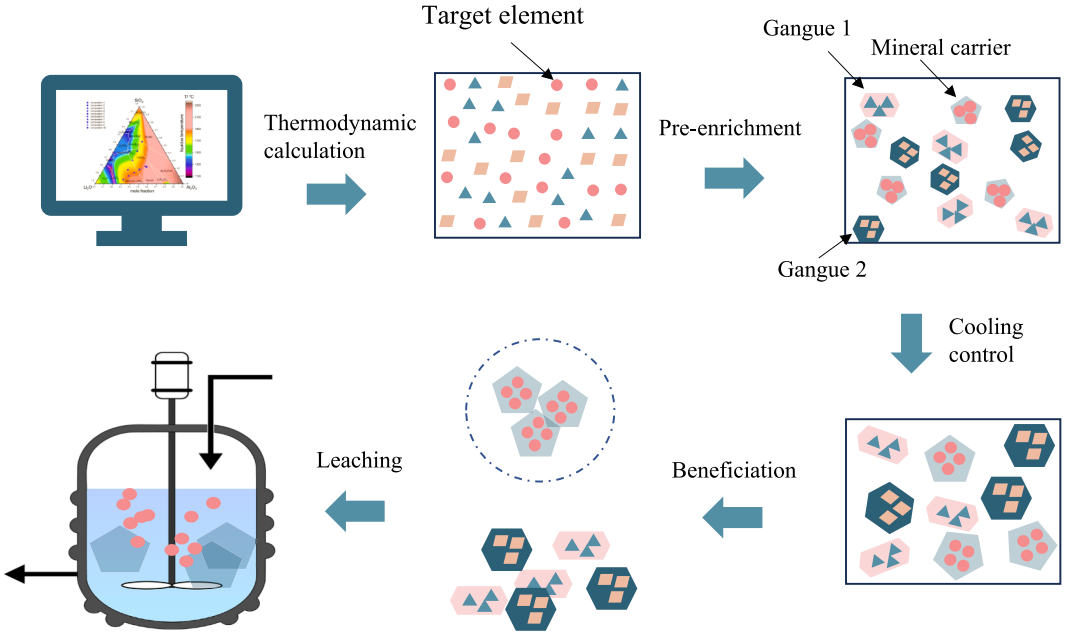

Fig. 1. Schematic sketch of the EnAM method.

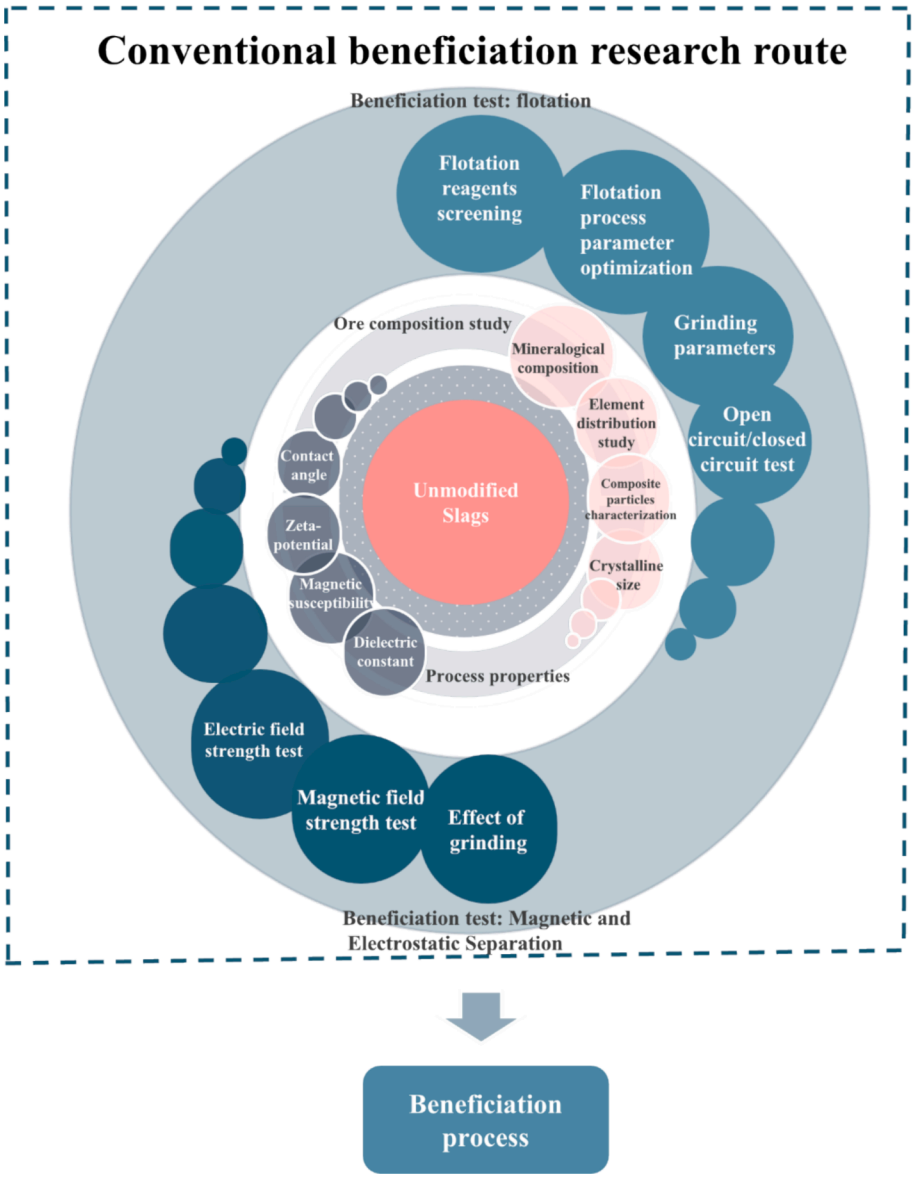

Fig. 2. Schematic drawing of conventional beneficiation research route for slag: experimental materials determine the beneficiation process.

target phase γ-lithium aluminate from a thermodynamic controlled slag, as well as the selective inhibition of the typical slag mineral gehlenite. This provides a deeper understanding and supplement to our previous micro-flotation research. Previous studies have demonstrated that fatty acid-based collectors, such as sodium oleate (NaOl), facilitated flotation recoveries surpassing 69 % for γ-lithium aluminate in micro-flotation trials. This material could also be floated using naphthenic acid and commercial collectors FS-2, FS-100, and SM-15 (Haas et al., 2018; Qiu et al., 2022; Qiu et al., 2021). Additionally, the potential for enriching γ-lithium aluminate from the slags has been explored (Haas et al., 2018). However, the lithium recovery is not sufficient and systematic flotation studies on Li-containing slag, such as research on factors affecting the flotation performance of slag, have not been conducted yet. In addition, in this paper, the leachability of the slag was also investigated and discussed.

2. Materials and experimental methods

2.1. Materials

The slag samples were produced by the Institute of Process Metallurgy and Metal Recycling (IME), RWTH Aachen University. Two slags were produced at different cooling rates. Sample S2_15kg was cooled at a rate of 50 °C/h, while sample S5_15kg was cooled at a rate of 25 °C/h and was additionally held at 1150 °C for 6 h. The melting experiments were conducted in a graphite crucible. 15 kg of synthetic slag for each sample was prepared with the compositions listed in Table 1. After chemical and mineralogical analysis, the slag samples were ground at the Institute of Particle Technology, TU Braunschweig.

γ-lithium aluminate (Sigma-Aldrich, Germany) and gehlenite (Vata de Sus, Hunedoara, Romania) were used for the characterization. The gehlenite was crushed and sieved; the undersized product, obtained from the 63 μm sieve, was employed for surface analysis. The sample underwent a series of analyses including chemical analysis (Supplementary Material Table S1), particle size measurement (Supplementary Material Figure S1), and X-ray powder diffraction analysis (XRD, Supplementary Figure S2). The XRD analysis revealed impurities such as merwinite, wollastonite, and calcite in addition to the major phase gehlenite. In our previous article, we referred to this mineral as the melilite solid solution (Qiu et al., 2021). However, according to Marince et al. (Marincea et al., 2011), solid solutions composed of end-member minerals like gehlenite and åkermanite can also be expressed as

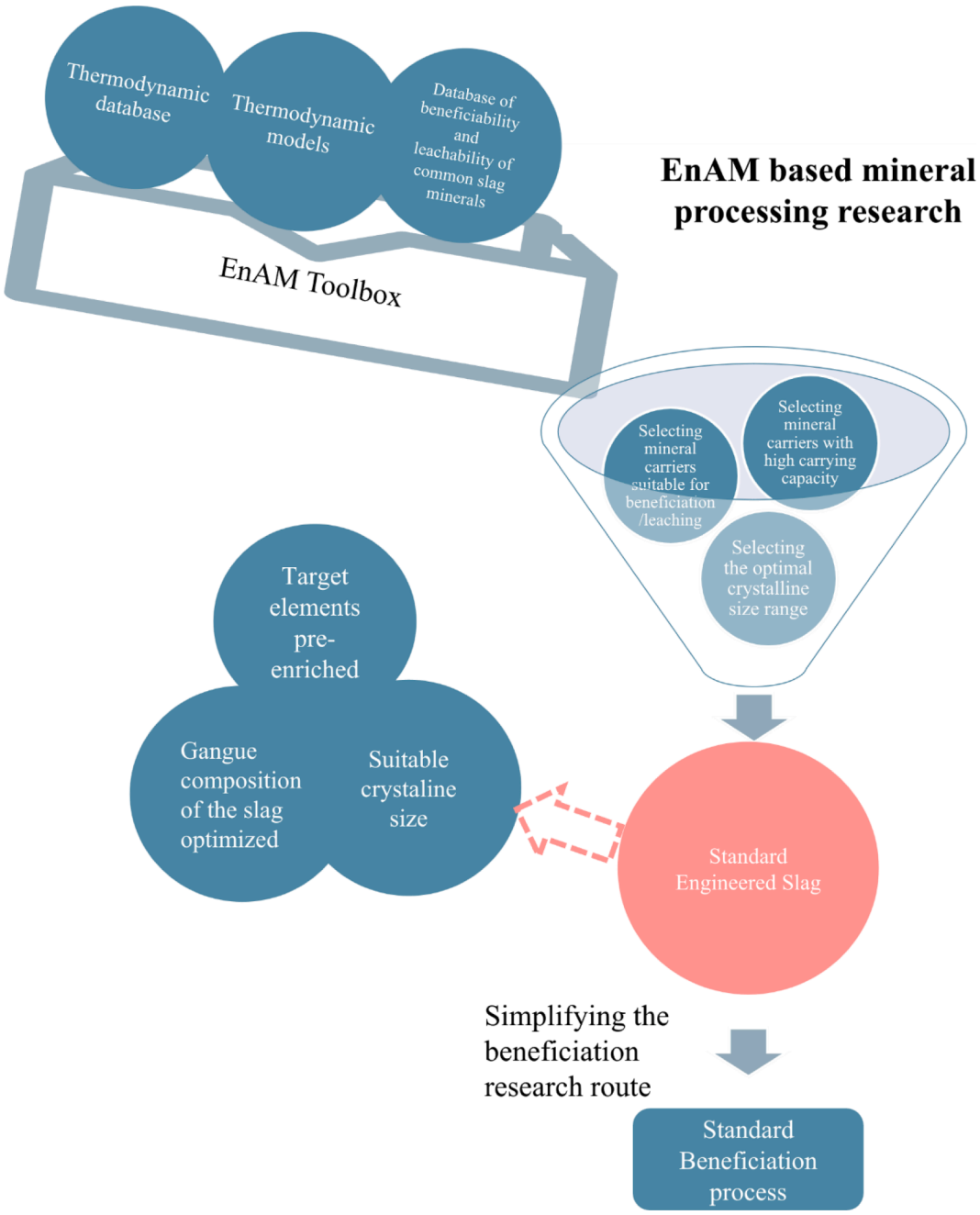

Fig. 3. EnAM strategy allows the process to determine the experimental materials, namely by engineering the slag to make it more adaptable to simplified beneficiation workflows. From this perspective, the workload of mineral processing research on slags can be significantly reduced.

Table 1
Weighed in composition of the slag samples and chemical composition of the slag samples in wt %.

	Sample	Al_2O_3	CaO	Li_2O	MnO	SiO_2
Weighed in composition of the slag samples in wt %	S2_15kg	39.7	16.9	11.6	5.3	26.5
	S5_15kg	46.4	22.5	10.1	6.0	15.0
Chemical composition of the slag samples in wt %	S2_15kg	37.6	16.2	9.3	5.0	28.9
	S5_15kg	43.6	22.1	8.8	5.4	18.4

gehlenite. Therefore, in this paper, we will use the term "gehlenite" to describe this mineral.

2.2. Chemical and mineralogical analysis

Qualitative x-ray diffraction analyses were performed on a D4 ENDEAVOR, BRUKER AXS GmbH at TU Clausthal, with Bragg-Brentano reflection geometry and Cu-Kα radiation (35 kV and 40 mA). The instrument is equipped with a fixed divergence slit, primary soller slit (2.5°), anti-scatter slits, a diffracted beam monochromator and a LynxEye-detector. The milled samples were transferred to the sample holder using the backloading method and measured in the angular range of 5° – 80° 2 θ with a step size of 0.0014° 2 θ and a measurement time of 0.02 sec per step.

Quantitative x-ray diffraction analyses were performed in reflective

geometry on a PANalytical X'Pert Pro MPD θ-θ diffractometer with Co-Kα radiation (40 kV and 40 mA) at BGR Hannover. The instrument is equipped with a programmable divergence slit (20 mm irradiated length) primary and secondary soller slits (0.04 rad), anti-scatter slits, a fixed incident beam mask (10 mm), a diffracted beam monochromator and a point detector. The milled samples were transferred to the sample holder using the backloading method and measured in the angular range of $5^\circ - 70^\circ$ 2 θ with a step size of 0.03° 2 θ and a measurement time of 15 sec per step. For the Rietveld refinement, the software Profex/BGMN (Version 5.1.0) (Doebelin and Kleeberg, 2015) with the included structure collection and additional crystal structure data from Pillars and Peacor (β-$LiAlSiO_4$) (Pillars and Peacor, 1973), Marezio (γ-$LiAlO_2$) (Marezio, 1965), Lager and Meagher ($CaMnSiO_4$) (Lager and Meagher, 1978), Politaev et al. (Li_2MnSiO_4) (V.V. Politaev et al., 2007) and Famery et al. ($LiAl_5O_8$) (Famery et al., 1979) was used. To determine the amorphous content an internal standard (20 wt% corundum, NIST No.676) was added to each powder sample. Microstructure analysis were also done at BGR in high vacuum at 20 kV on polished, carbon coated samples embedded in epoxy resin using a FEI MLA 650F Quanta FEG scanning electron microscope (SEM). The device is equipped with a field emission gun and various detectors (e.g. BSE detector, two (EDS) silicon drift detectors) for standardless semi-quantitative element analysis.

The elemental content of slag samples and liquid samples were measured by an ICP optical emission spectrophotometer (ICP-OES 5100, Agilent, Agilent Chemical Bulk Analysis Technologies Germany GmbH & Co. KG, Waldbronn, Germany) at TU Clausthal. Samples were melted with lithium tetraborate in a platinum crucible at 1050 °C, and then leached with dilute hydrochloric acid to measure the content of aluminum, calcium, magnesium, manganese and silicon. To measure lithium and other elements, the samples were mixed with nitric acid and digested at 250° C and under a pressure of 80 bar in an autoclave (TurboWAVE, MLS, Leutkirch im Allgäu, Germany). Following filtration, drying, and weighing, flotation products were sampled for chemical element analysis to ascertain the recovery. The flotation recoveries were computed using the below Equation (Drzymała and Swatek, 2007):

$$\varepsilon = \frac{\gamma \bullet \lambda}{\alpha} \tag{1}$$

where ε is the recovery of a component; γ is the yield of a product; λ is content of a component in a product; α is content of a component in the feed.

2.3. Thermodynamic modeling

In this study, basic thermodynamic models and FT-Oxide database directly from commercial software Factsage 8.2 (Bale et al., 2016) is employed within the Calculation of Phase Diagram (CALPHAD) framework (Lukas et al., 2007) (Saunders and Miodownik, 1998). This approach is used to calculate and design the composition of the slag before producing slag for subsequent flotation and chemical leaching. The prediction of the solidified phases of each sample, as well as the solidification process, is carried out under equilibrium conditions. Additionally, the amounts of solidified phases are calculated when the liquid phase has just disappeared.

2.4. Flotation

Flotation experiments on the slag were executed using a 125 mL Denver-type flotation machine configured in an IFAD construction (Fig. 4A). The agitation speed was set at 2000 rpm, and the airflow rate sustained at 40 L/h. Each trial required a 20 g slag sample. The sample was inserted into the flotation cell, filled with distilled water, and agitated for one minute prior to the introduction of reagents. The conditioning period for each reagent was set at one minute, with a flotation scraping time of five minutes. Upon conclusion of the experiment, the flotation products underwent filtration, drying, and weighing procedures, followed by subsequent XRD and elemental analysis.

Sodium oleate (Riedel-de-Haën) was employed as the collector. The frother is pine oil (American Cyanamid/Cytec). Sodium hexametaphosphate (ThermoFisher Scientific) was used as a modifying reagent. An emulsifier (Emulsogen, Hoechst/Clariant, Germany) was added to the frother pine oil in a mass ratio of 1:10 and was diluted to a 1 wt% emulsion for use.

2.5. Leaching

Leaching tests were conducted in a beaker under conditions of a liquid-to-solid ratio of 25:1, leaching time of 90 min, and agitation speed of 400 rpm. The study primarily examined the impact of the acid concentration and the temperature on the leaching efficiency and selectivity.

2.6. Surface characterization analysis

The Zeta potential of the sample was assessed utilizing a Zetasizer Nano (Malvern) at TU Clausthal. The mineral sample was positioned within a 500 mL measuring cylinder and introduced with 500 mL of

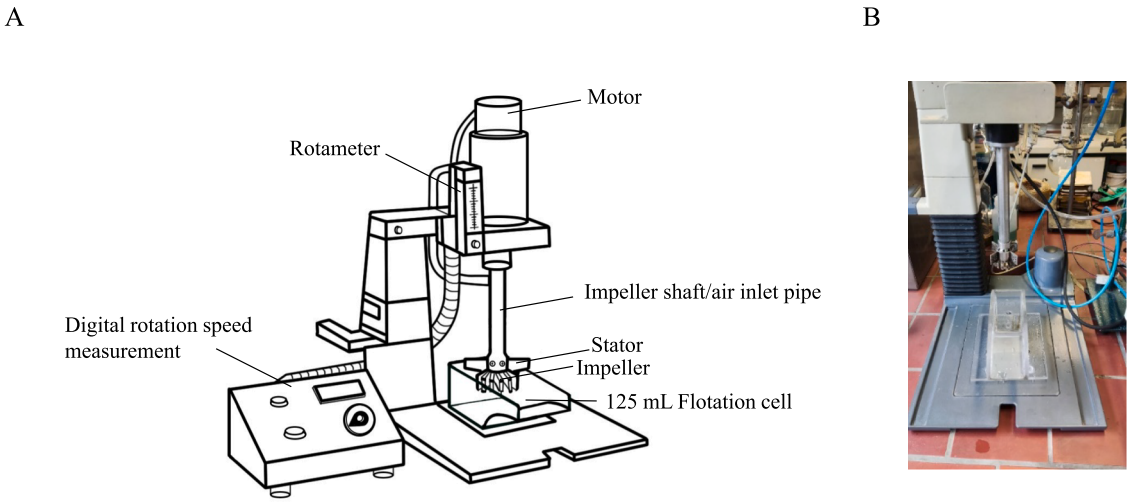

Fig. 4. A. Sketch of IFAD-construction Denver-type flotation machine. B. Picture of IFAD-construction Denver-type flotation machine.

distilled water, subsequently sealed with a plastic film atop the cylinder. The cylinder was agitated ten times and left to settle for one hour. The supernatant was collected for the Zeta potential measurement. The pH was manipulated using HCl and NaOH, respectively. Powder contact angle measurements were conducted employing the Washburn method, utilizing a tensiometer (DCAT25, Data Physics) as the measurement apparatus.

3. Results and discussion

3.1. Slag design with thermodynamic tools

In previous lithium-containing slag systems, such as the Li_2O-Al_2O_3-SiO_2-CaO-MgO slag system (Li et al., 2022; Schirmer et al., 2020), as well as high-aluminum slags from spent LIBs (Elwert et al., 2012) and artificial mineral slags derived from black mass (Sommerfeld et al., 2020), the distribution of lithium has been observed and confirmed in various lithium-containing silicates and oxides, including β-eucryptite, spodumene, lithium-containing spinel solid solution and γ-lithium aluminate. The extensive dispersion of lithium across various phases presents challenges in downstream processing and the efficient recovery of lithium from slag. This highlights the need for designing the composition of slags to facilitate the enrichment of lithium in a single target phase, such as γ-lithium aluminate. In this study, thermodynamic simulations were performed. Moreover, internal mass fraction of three main slag matrix components CaO, SiO_2 and Al_2O_3 were designed as 20 wt%, 32 wt% and 48 wt% respectively. These were derived from the real battery slag, such as Umicore battery slag (Elwert et al., 2012). The content of Li_2O and MnO varied within practical ranges, specifically ranging from 6 wt% to 11 wt% for Li_2O and from 0.5 wt% to 10 wt% for MnO. Here, the solidified phases of four samples S1(p), S2(p), S3(p), S4(p), which are presented in Fig. 5 were calculated under the equilibrium condition, where the liquid slag phase just disappeared. Since the solid reactions in the high viscosity slag system are extremely slow, their reaction processes were disregarded under the cooling rate of 50 °C/h.

Based on the thermodynamic simulation, the main solidified phases within the slags were gehlenite, β-eucryptite and γ-lithium aluminate. In samples S2(p) and S4(p), the amount of glaucochroite was also significant. In this set of samples, the mass fraction of the target product γ-lithium aluminate was higher in sample S2(p) than that of the other samples, reaching 28 wt%. Consequently, for reaching increased amounts of the target product γ-lithium aluminate, the initial composition of sample S2(p) was considered suitable. This composition served as a starting point for subsequent slag production to assess the efficiency of lithium recycling using froth flotation and chemical leaching.

Excessively fine γ-lithium aluminate crystals could potentially compromise their complete liberation after grinding, thereby affecting subsequent flotation efficiency. Therefore, consideration should be given to reducing the cooling rate and achieving a coarser crystal size while designing the slag. It is also crucial to enrich lithium in the form of γ-lithium aluminate while minimizing the presence of other lithium-containing phases such as β-eucryptite. Based on that, an additional slag was designed, and the slag composition was further adjusted by incorporating appropriate quantities of fluxes, such as CaO and SiO_2. In the previous study, the average contents of Li_2O, MnO as well as Al_2O_3 in the above samples were utilized as fixed internal mass fraction (Ranneberg et al., 2023). At the same time, the addition of SiO_2 and CaO were varied from 15 wt% to 30 wt%. These requirements served as constraint conditions of thermodynamic modelling to seek for the re-designed slag composition. Based on the thermodynamic calculation, a trend could be observed where an increase in the amount of CaO and a decrease in the amount of SiO_2 in the input led to an upward trend in the content of gehlenite, while the content of eucryptite was reduced. When the initial composition reached that shown in Fig. 6, and the liquid phase was just disappeared, lithium was exclusively incorporated into the target phase γ-lithium aluminate, with the γ-lithium aluminate content at approximately 45 wt%, and the content of eucryptite was 0. Furthermore, the content of gehlenite increased to about 32 wt%. This implied that, theoretically, complete transfer of lithium into the target phase the γ-lithium aluminate was feasible. In Fig. 6, the corresponding equilibrium solidification process was also predicted. When the slag temperature was over 1432 °C, this slag system was completely in liquid state. As the temperature decreased, γ-lithium aluminate as primarily crystalline was precipitated followed by $CaAl_2O_4$ and dominant matrix phase of solidified slag: gehlenite. Towards the end of the solidification process, Mn-containing phases, such as Mn-Al spinel solid solution, MnO and glaucochroite, were expected to precipitate.

Consequently, this slag composition S5(p) was employed for the upscaling production. Moreover, experimental verification was conducted,

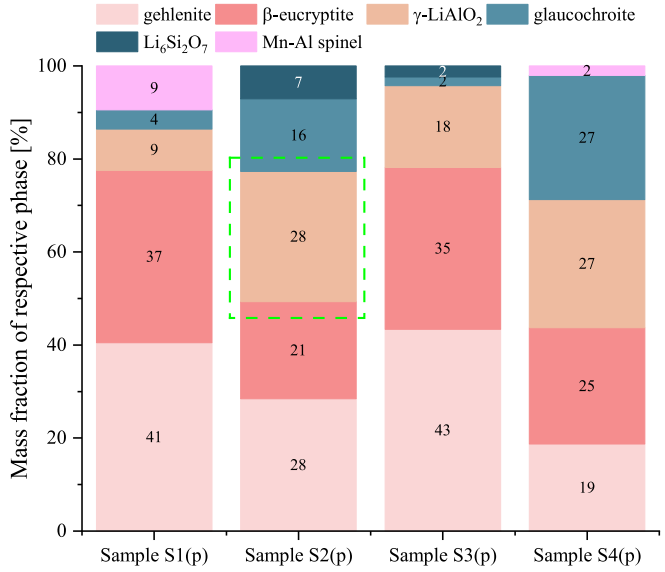

Fig. 5. Predicted solidified phases of the samples S1(p), S2(p), S3(p) and S4(p) under equilibrium condition at 1 atm. Different solidified phases are marked in the legend and labelled in mass fraction. The highest amount of γ-lithium aluminate in sample S2(p) is marked with the green dashed rectangular. (For interpretation of the references to colour in this figure legend, the reader is referred to the web version of this article.)

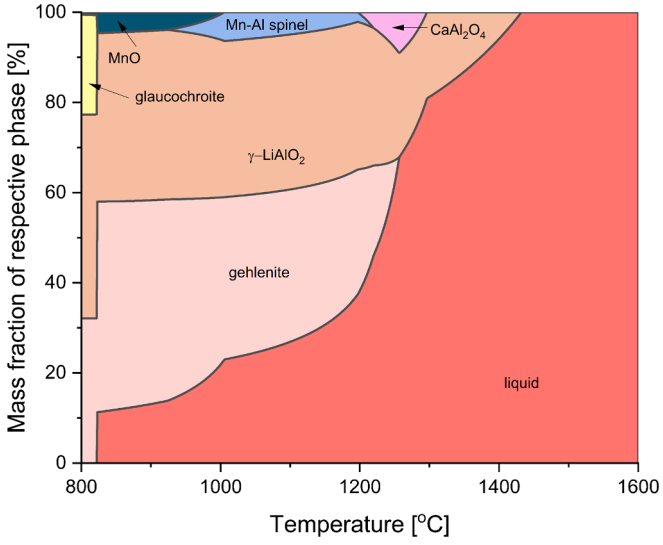

Fig. 6. Calculated equilibrium solidification process of the re-optimized sample S5(p) with the initial composition: Li_2O: 10.1 wt%, Al_2O_3: 46.4 wt%, SiO_2: 15.0 wt%, CaO: 22.5 wt%, MnO: 6.0 wt%.

followed by flotation and chemical leaching processes to assess the efficiency of lithium recycling.

3.2. Chemical and mineralogical characterization of the slags

The chemical composition of the investigated slag samples S2_15 kg and S5_15 kg is shown in Table 1. Compared to the weighed in composition of the slag, the content of aluminum and lithium has decreased. This may be due to the evaporation of lithium during high-temperature smelting (Schirmer et al., 2020).

Table 2 shows the Rietveld quantitative phase analysis of the investigated slags. The results prove that both samples contained large amounts of amorphous components. In addition, five crystalline phases from the mineral groups of silicates and oxides were quantified. Three of them contained lithium: γ-lithium aluminate (γ-$LiAlO_2$), β-eucryptite (β-$LiAlSiO_4$) and lithium manganese silicate (Li_2MnSiO_4), two slag phases were lithium free: gehlenite ($Ca_2Al_2SiO_7$) and glauchochroite ($CaMnSiO_4$). The main phases included gehlenite, γ-lithium aluminate, amorphous constituents and also β-eucryptite in the sample S2_15kg. A comparison of the quantitative phase composition with the predicted equilibrium solidification (Fig. 5 and Fig. 6) reveals, that most of the phases were correctly predicted by the thermodynamic model, except for lithium manganese silicate and the amorphous constituents. This inconsistency is due to the fact that amorphous phases cannot be considered under equilibrium conditions and the thermodynamic properties of lithium manganese silicate are missing in the FT-Oxide database.

Studies of grain size, crystal morphology and degree of intergrowth of the slag phases were carried out using a scanning electron microscope (SEM) at BGR. The results show that the slag samples were solidified in a compact, heterogeneous, hypocrystalline, fine- to medium-grained, polycrystalline microstructure (Fig. 7 A and B). In both slags, euhedral to skeletal or dendritic crystals of variable size lie in a matrix of glassy solidified residual melt. The sample S2_15 kg, cooled down with 50 °C/h, contained predominantly skeletal to dendritic crystallised phases. The grain size of the gangue phase gehlenite in this slag was in the range of < 20 μm to 200 μm, while the target phase γ-lithium aluminate reached grain sizes between 10 μm to > 1 mm. In contrast, gehlenite was subhedral and γ-lithium aluminate was euhedral crystallized in the sample S5_15 kg, produced with a hold time of 6 h at 1150 °C and a cooling rate of 25 °C/h. The grain sizes of gehlenite and γ-lithium aluminate ranged in this slag from 100 μm to > 1 mm and 20 μm to > 500 μm, respectively. β-Eucryptite was characterized by fine subhedral crystallites with grain sizes of < 30 μm. The amorphous phases appeared in the samples in form of glassy solidified residual melt in the crystal interstices. Finely dispersed, closely intergrown, dendritic to net-like aggregates of glaucochroite were present in the amorphous components.

The microstructure studies indicate that the manganese-containing phase glaucochroite crystallized after the lithium-containing phases and gehlenite when the melt solidified. This observation is consistent with earlier studies (Ranneberg et al., 2023).

Table 2
Rietveld quantitative phase analyses of the slag samples S2_15 kg and S5_15 kg in wt %. Agreement indices R_{wp} and R_{exp} are given in %. Values in parentheses represent twice the estimated standard deviations (2σ) reported by BGMN.

	S2_15 kg	S5_15 kg
gehlenite	25.9 (1.2)	38.7 (1.3)
γ-$LiAlO_2$	25.4 (1.7)	27.4 (1.0)
glaucochroite	2.9 (1.2)	4.1 (0.4)
Li_2MnSiO_4	5.8 (0.5)	3.8 (0.4)
β-eucryptite	11.4 (0.9)	2.2 (0.2)
amorphous	28.6 (1.7)	23.8 (2.4)
R_{wp}	6.92	8.73
R_{exp}	4.33	5.30
χ^2	2.55	2.71

3.3. Flotation experiments: Effect of particle size on flotation

The slag sample S2_15kg was crushed to a particle size of < 500 μm followed by dry sieving. The sample was divided into three particle size fractions: <32 μm, 32–100 μm and > 100 μm. Flotation tests were performed on these fractions to investigate the effect of the particle size on flotation results. The particle size distributions for these three fractions are illustrated in Fig. 8A. Fig. 8B shows the particle size distribution of the slag after being dry ground for 30 s.

The anionic collector NaOl was used for the flotation tests based on previous micro-flotation tests (Qiu et al., 2021). Since the highest yield of γ-lithium aluminate is obtained under the natural pH around 11 in micro-flotation tests (Qiu et al., 2021), the pH of the flotation slurry was not adjusted throughout the experiments, and its natural pH was about 10–11.

Starting with the coarse particle size fraction, >100 μm, no significant enrichment of Li in the flotation concentrate was observed, and the yield was only 43.8 % (Table 3). This indicated that in this particle size fraction, the target phase γ-lithium aluminate was not sufficiently liberated after grinding, resulting in the accompanying gangue minerals also entering the flotation concentrate, leading to poor selectivity.

In the case of the fraction 32–100 μm and < 32 μm, an enrichment of Li in the flotation concentrate was observed. In the flotation concentrate of 32–100 μm fraction, the Li_2O content could be increased to around 12 wt%, while the Li_2O content in the tailings decreased to about 8.2 wt%. Moreover, in these two fractions, the recovery of Li in the flotation concentrate reached 74 %-85 %. This also reflected the collecting capability of NaOl for γ-lithium aluminate – not only did it exhibit good collecting ability of NaOl for γ-lithium aluminate in micro-flotation, but it also showed the same in slag flotation. However, the lithium content in the flotation tailings of these two particle size fractions remained unsatisfactorily high, which could be caused by poorly liberated fine γ-lithium aluminate crystals. The quantity of these finely dispersed γ-lithium aluminate crystals that are difficult to liberate, and it can only be reduced by optimizing the slag design and cooling regime. Furthermore, the calcium content, which is a tracer element of gehlenite, revealed that the calcium content in the concentrate has been significantly lower than that in the tailings, although the gehlenite content in the concentrate was still high.

Conversely, after the slag has been ground by the disc mill, it became entirely non-floatable. It is hypothesized that difficulties in flotation could be caused by slime coating, potentially caused by overly fine particle sizes or caused by the slime coating of gangue mineral gehlenite.

The crushed slag S5_15kg was also dry sieved and divided into three particle size ranges: < 32 μm, 32–100 μm, and > 100 μm. The particle size analysis of these fractions is shown in Fig. 9.

Flotation tests were conducted on samples from each fraction. The flotation results are shown in Table 4. The flotation performance of this slag is overall lower than that of the slag sample S2_15kg. Notably, the > 100 μm fraction was entirely non-floatable. Even after the > 100 μm fraction was dry ground for 5 s and 30 s in a disc mill prior to flotation, it still remained non-floatable (Table 5). However, after the 32–100 μm fraction was wet sieved again to de-slime, the flotation yield increased to about 95 %. Similarly, after grinding and wet sieving the > 100 μm fraction using a 32 μm sieve, the flotation yield also increased to about 96 %. It indicates that wet sieving and de-sliming directly affect the flotation yield of the slag. Nevertheless, a too high flotation yield implies that both the target mineral particles and gangue mineral particles have entered the froth product, indicating that this flotation process is unable to achieve the intended separation.

3.4. Flotation experiments: Effect of the dosage of SHMP on flotation

To enhance the purity of the flotation concentrate, further suppression of gehlenite is a crucial strategy for improving the purity of γ-lithium aluminate in the flotation concentrate. During the flotation

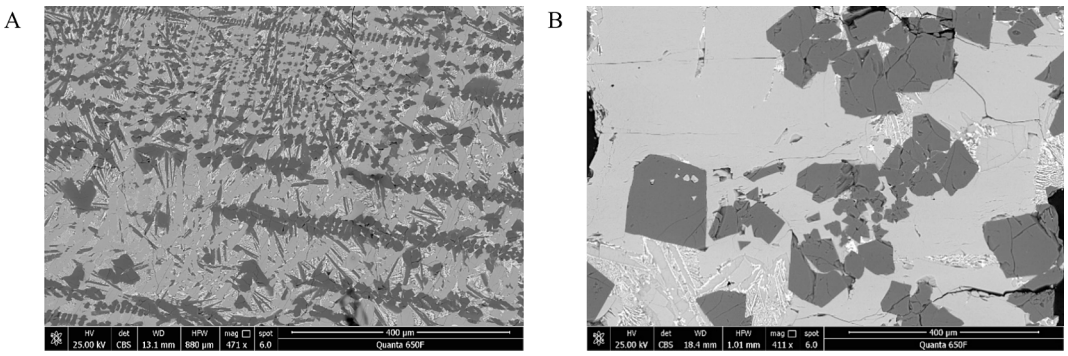

Fig. 7. Backscattered electron (BSE) images of the microstructure of sample S2_15 kg (A) and sample S5_15 kg (B). dark grey = γ-lithium aluminate, light grey = gehlenite, white = mixture of glaucochroite in an amorphous/ glassy residual melt.

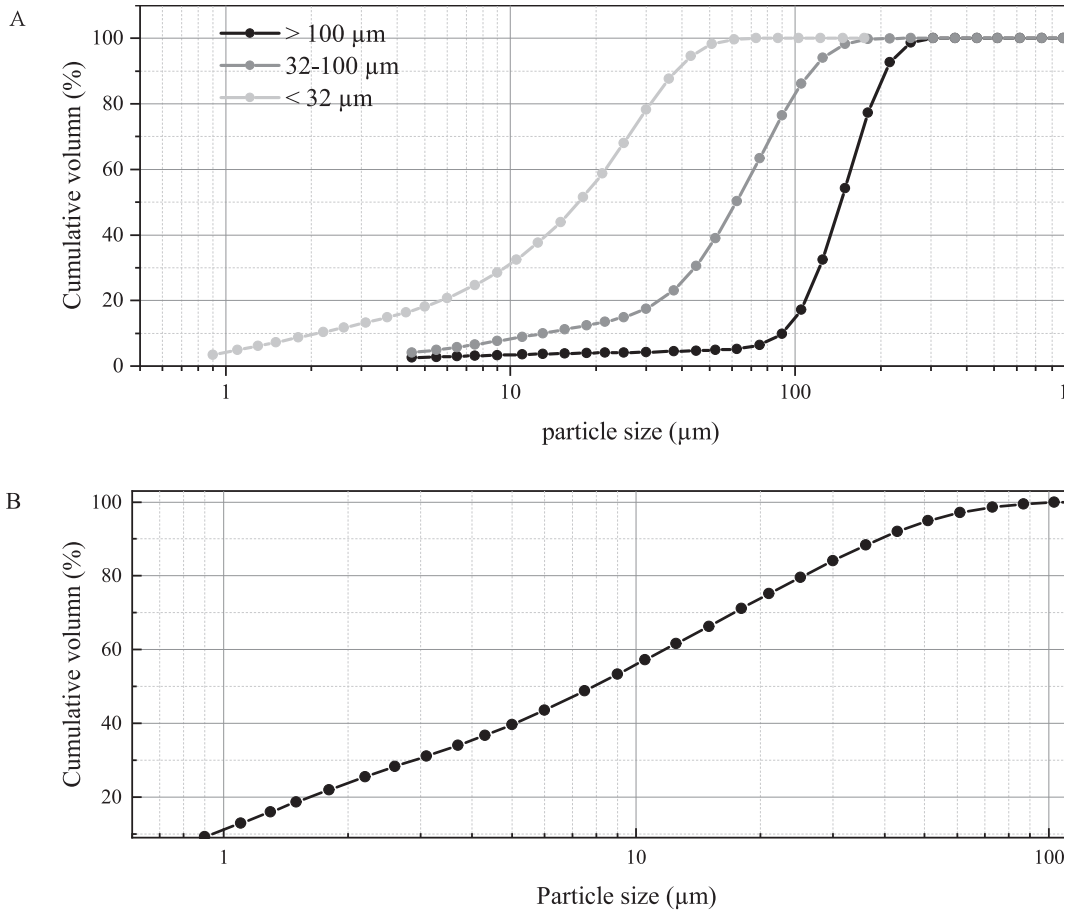

Fig. 8. A. Particle size distribution of the fractions > 100 µm, 32–100 µm and < 32 µm of slag sample S2_15kg. B. Particle size distribution of slag sample S2_15kg after dry grinding for 30 s.

trials involving diaspore and kaolinite, with a NaOl system, it is observed that sodium hexametaphosphate (SHMP) could activate diaspore while inhibiting the flotation of kaolinite under neutral and alkaline conditions (Zhang et al., 2018). Thus, in this paper, we also investigated the use of SHMP to inhibit gehlenite.

The results of sample S2_15kg (fraction 32–100 µm), illustrated in Table 6, prove/show that an increasing dosage of SHMP lead to an increasing Li_2O content in the concentrate from about 12 wt% to 14.4 wt %. Moreover, the CaO content in the concentrate gradually decreased from 12.9 wt% to 7.8 wt% after the addition of SHMP. Hence, the addition of SHMP effectively enhanced the purity of the γ-lithium aluminate concentrate. In addition, lithium recovery in the concentrate decreased with increasing SHMP dose. This might be due to SHMP also inhibiting the up-floating of γ-lithium aluminate to a certain extent. In the flotation process design, the recovery of Li in concentrate can be further augmented by adding scavenger stages.

The enrichment of lithium in the concentrate is also supported by the XRD data. As both γ-lithium aluminate and β-eucryptite contain lithium, determining the exact enrichment of these two mineral phases by elemental analysis alone is a significant challenge. As a result, qualitative XRD analysis was introduced to assist in delineating the mineral phase enrichment. This was achieved by comparing the intensity of the major diffraction reflex of the mineral phases.

As shown in Fig. 10, with a SHMP dosage of 0 g/t, there was a

Table 3
Flotation results of sample S2_15kg, using NaOl as an anionic collector.

Fraction	Part of the sample	Flotation yield, %	Li_2O content, wt %	Li recovery, %	CaO content, wt %	Ca recovery, %
> 100 μm	Concentrate	43.81	9.06	45.14	16.99	42.53
	Tailing	56.19	8.59	54.86	17.90	57.47
	Feed	100.00	8.80	100.00	17.50	100.00
32–100 μm	Concentrate	79.73	11.99	85.22	12.97	73.06
	Tailing	20.27	8.18	14.78	18.82	26.94
	Feed	100.00	11.22	100.00	14.16	100.00
< 32 μm	Concentrate	64.03	12.25	74.21	12.06	52.94
	Tailing	35.97	7.58	25.79	19.09	47.06
	Feed	100.00	10.57	100.00	14.59	100.00
−500 μm, Dry grinding 3 s in disk mill			Non-floatable			
−500 μm, Dry grinding 5 s in disk mill			Non-floatable			
−500 μm, Dry grinding 30 s in disk mill			Non-floatable			

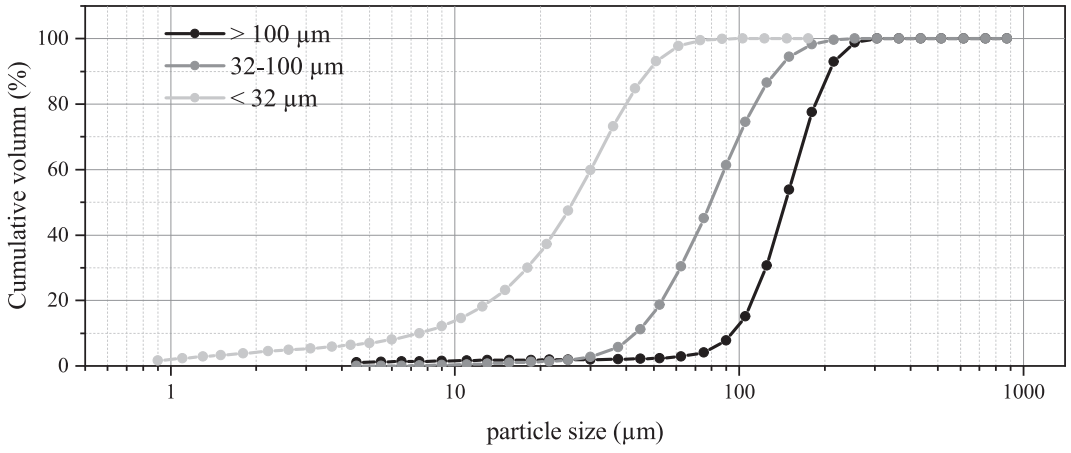

Fig. 9. Particle size distribution of the fractions > 100 μm, 32–100 μm and < 32 μm of slag sample S5_15kg.

Table 4
Flotation results of S5_15kg across different particle size fractions. using NaOl as an anionic collector.

Fraction	Part of the sample	Flotation yield, %	Li_2O content, wt. %	Li recovery, %	CaO content, wt. %	Ca recovery, %
< 32 μm	Concentrate	61.61	11.69	67.59	14.13	53.93
	Tailing	38.39	9.00	32.41	19.38	46.07
	Feed	100.00	10.66	100.00	16.15	100.00
32–100 μm	Concentrate	14.01	–	–	–	–
>100 μm	Concentrate	Non-floatable	–	–	–	–

Table 5
Flotation results of S5_15kg after wet sieving and S5_15kg after different grinding times.

Experimental conditions	Fraction	Flotation yield
32–100 μm wet sieving	Concentrate	95.40
>100 μm, Dry grinding 5 s in disk mill	Concentrate	Non-floatable
>100 μm, Dry grinding 30 s in disk mill	Concentrate	Non-floatable
Grinding of the > 100 μm fraction to < 100 μm and desliming through a wet sieving	Concentrate	95.75

significant enrichment of γ-lithium aluminate in the flotation concentrate. However, gehlenite did not show enrichment in the flotation tailings, instead, it was distributed in both the concentrate and tailings. When the SHMP dosage was raised to 500 g/t, the content of gehlenite in the concentrate markedly decreased. This effectively demonstrates the suppression effect of SHMP on gehlenite.

However, the effect of SHMP on β-eucryptite flotation was not significant. Therefore, the influence of β-eucryptite should be fully considered, if the aim is to further increase the purity of γ-lithium aluminate in the concentrate or to reduce lithium losses in the tailings. For example, the β-eucryptite content can be reduced from the mineral composition of the slag through strategic slag design or additional research can be pursued concerning the floatability of β-eucryptite.

The effect of SHMP dosage (50–200 g/t) on flotation was also conducted for slag S5_15kg. In Section 3.3, it is mentioned that slag with a particle size greater than 100 μm, after being ground to below 100 μm and subjected to wet sieving with a 32 μm sieve, can achieve a flotation yield of up to about 96 %. Therefore, it is necessary to use inhibitors to reduce the up-floating of the gangue mineral gehlenite. Prior to the flotation tests, the test material was subjected to wet sieving desliming. The results are shown in Supplementary Material Table S2 and follow a similar trend to the experimental results for slag sample S2_15 kg. It can also be observed that SHMP has an inhibitory effect on gehlenite. As shown in Fig. 11, by adding a cleaner stage, the purity of γ-lithium aluminate concentrate can be improved compared to the results in Table 4 and Table 5, and the up- floating of gehlenite can be further inhibited (Table 7).

Table 6
Flotation results of sample S2_15kg after dosage of SHMP.

dosage of SHMP	Part of the sample	Flotation yield, %	Li_2O content, wt %	Li recovery, %	CaO content, wt %	Ca recovery, %
0 g/t	Concentrate	88.30	11.97	92.51	12.90	82.53
	Tailing	11.70	7.32	7.49	20.61	17.47
	Feed	100.00	11.43	100.00	13.80	100.00
200 g/t	Concentrate	38.62	12.87	43.64	11.33	31.43
	Tailing	61.38	10.46	56.36	15.56	68.57
	Feed	100.00	11.39	100.00	13.92	100.00
300 g/t	Concentrate	37.64	12.79	42.60	10.96	29.75
	Tailing	62.36	10.40	57.40	15.62	70.25
	Feed	100.00	11.30	100.00	13.87	100.00
500 g/t	Concentrate	25.92	14.38	32.84	7.79	14.18
	Tailing	74.08	10.29	67.16	16.51	85.82
	Feed	100.00	11.34	100.00	14.24	100.00

3.5. Surface property analysis

The Zeta potential is an electrical potential within the interfacial double layer at the location of the slipping plane (Drzymała and Swatek, 2007; Tian et al., 2018). Serving as an indicator of the potential alteration at the particle surface, it proves a valuable instrument for indirectly assessing the interaction of flotation reagents with the particle surface in pulp solutions (Feng et al., 2018). The Zeta potentials of γ-lithium aluminate and gehlenite were measured under various conditions by adjusting the slurry pH within a range of 2 to 12. The results of this analysis are illustrated in Fig. 12.

Firstly, within the measured pH range, both γ-lithium aluminate and gehlenite exhibited negative charges in distilled water. In the presence of a NaOl solution, the potential of both γ-lithium aluminate and gehlenite underwent negative shifts to varying degrees, indicating that both γ-lithium aluminate and gehlenite could adsorb the oleate ions. This also explains why gehlenite still existed in the flotation concentrate. However, the magnitude of the negative shift in zeta potential of gehlenite is smaller over most of the pH range.

After the addition of SHMP, the Zeta potential of gehlenite underwent an overall negative shift, and the magnitude of this shift was even greater than that seen with NaOl. This indicates that, compared with NaOl, SHMP is more readily adsorbed on the surface of gehlenite. Upon the addition of SHMP and NaOl, the Zeta potential of gehlenite was close to the potential when SHMP was added alone within the pH range of 5 to 11. It suggests that in this pH range, when SHMP and NaOl are present together, gehlenite would preferentially adsorb SHMP.

Following adding SHMP to γ-lithium aluminate, the Zeta potential of γ-lithium aluminate also negatively shifted, but the magnitude was even smaller than that of NaOl. This indicates that NaOl is more readily adsorbed onto the surface of γ-lithium aluminate. When adding both SHMP and NaOl to γ-lithium aluminate, the surface potential of γ-lithium aluminate was further shifting negatively and closed to that of NaOl, indicating that NaOl plays a more important role than SHMP in the adsorption onto γ-lithium aluminate in the measured pH range.

To further demonstrate the selective inhibitory effect of SHMP on gehlenite in a NaOl system, the powder contact angle of γ-lithium aluminate and gehlenite was measured respectively.

Flotation leverages the differences in hydrophobicity among mineral particles to effectuate the separation of distinct particles. The hydrophobicity degree of mineral particles can be characterized via the measurement of their contact angle (Drzymała and Swatek, 2007). Typically, the contact angle on a mineral surface can be measured by methods such as the sessile drop technique. However, due to factors such as surface roughness, swelling, and liquid penetration into the pores, the measurement of the contact angle for powders becomes quite challenging using these methods (Alghunaim et al., 2016). Therefore, in this case, indirect methods have been used to measure powder contact angles by relating the penetration rate or pressure (Drzymała and Swatek, 2007). The Washburn method was adopted to indirectly measure the powder contact angles of γ-lithium aluminate and gehlenite in this study.

The results (Table 8) revealed that the natural powder contact angle of γ-lithium aluminate is smaller than that of gehlenite. With the addition of 10^{-5} M sodium oleate, the powder contact angle of γ-lithium aluminate increased to 88°, while that of gehlenite increased to 71°. This suggests that at the same concentration, sodium oleate has a stronger adsorption capability for γ-lithium aluminate than for gehlenite. After adding 10^{-6} M SHMP, the contact angle of γ-lithium aluminate remained essentially unchanged, while that of gehlenite decreased dramatically. As the SHMP concentration was further increased to 10^{-5} M, the powder contact angle of γ-lithium aluminate started to decrease, dropping from 90° to 72°, while the decrease for gehlenite was more substantial, with the contact angle dropping to 11°. As the concentration of SHMP increased up to 10^{-4} M, the powder contact angle of γ-lithium aluminate continued to slowly decrease, while the contact angle of gehlenite decreased to the lower limit of the measurement.

From these results, it is clear that with the addition and increasing concentration of SHMP, the hydrophilicity of both γ-lithium aluminate and gehlenite began to increase. However, the hydrophilicity of gehlenite dramatically increased, while γ-lithium aluminate continued to maintain a certain degree of hydrophobicity. These results also corroborate the selective inhibitory effect of SHMP on gehlenite from another perspective.

3.6. Leaching behaviors of the slag samples

This study further compared the direct leaching of slag samples and the leaching effect of flotation concentrate. The concentration of Si in the leachate plays a significant role in hydrometallurgical processes. Excessive silicon concentrations can lead to the formation of silica gel (Davris et al., 2017; Ma et al., 2019; Voßenkaul et al., 2017), thus complicating filtration and causing pipe blockage. As demonstrated in Fig. 13A, a noticeable decrease in Si content within the leachate can be observed in the concentrate acquired through flotation. This indicates the direct impact of pre-separating aluminate and silicate by flotation on reducing the Si concentration in the leachate.

In Fig. 13B, the Si concentration in the leachate from the direct leaching of slag S5_15kg is significantly lower than that in the leachate from slag S2_15kg. This might be due to the inherently lower Si content in the S5_15kg slag itself. Moreover, the Si concentration in the leachate from the flotation concentrate of the S5_15kg slag is slightly lower than that in the leachate from its direct leaching. The mineralogical composition of the slag residue from leaching under various leaching conditions is presented in Supplementary Material Table S3.

4. Conclusion

This study introduces an approach to slag treatment whereby slags can be designed for easier beneficiation by using the EnAM method, thereby reducing the workload in mineral processing research. The core of the EnAM method lies in the development of robust thermodynamic

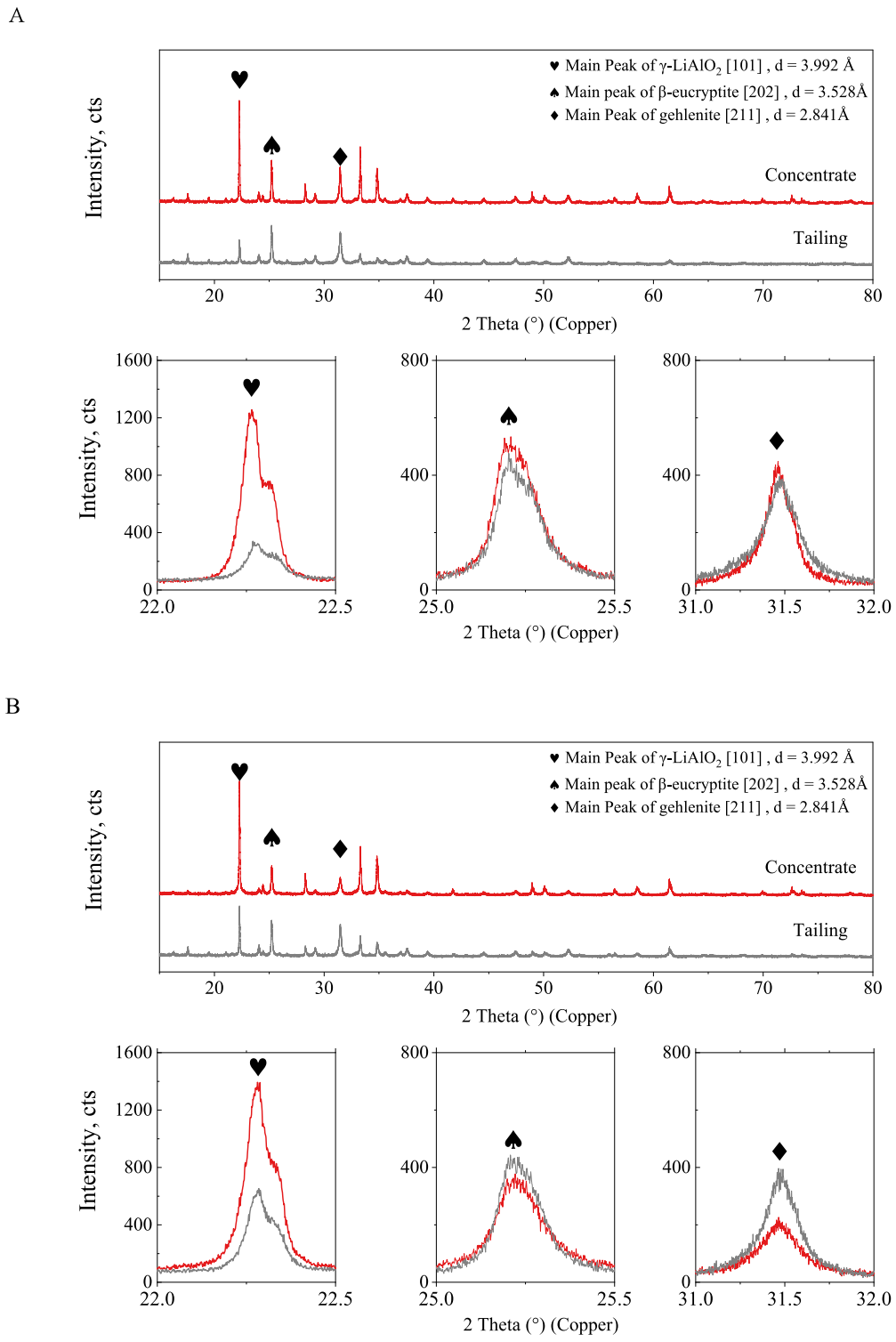

Fig. 10. XRD patterns of flotation concentrate and flotation tailings of S2_15kg when SHMP dosage is 0 g/t (A) and XRD patterns of flotation concentrate and flotation tailings of S2_15kg when SHMP dosage is 500 g/t (B).

databases and models, along with a thorough understanding of the processing properties of typical slag minerals, such as their floatability and leachability.

In this study, slag systems were designed consisting of the Li_2O-CaO-Al_2O_3-SiO_2-MnO system. Utilizing existing commercial thermodynamic databases and models, most of the lithium was successfully transferred to the γ-lithium aluminate phase, thereby reducing lithium dispersion. However, discrepancies remain between the thermodynamic predictions and the actual composition of the slag, indicating a need for further optimization of the thermodynamic database. In addition, an initial attempt was made to apply this strategy to the flotation study, and the research on flotation properties of lithium-containing slag is an important supplement to the technological path of high temperature pyrometallurgical recycling of spent LIBs.

It is found that the slag composition designed and predicted through the EnAM method is already close to the mineralogical composition

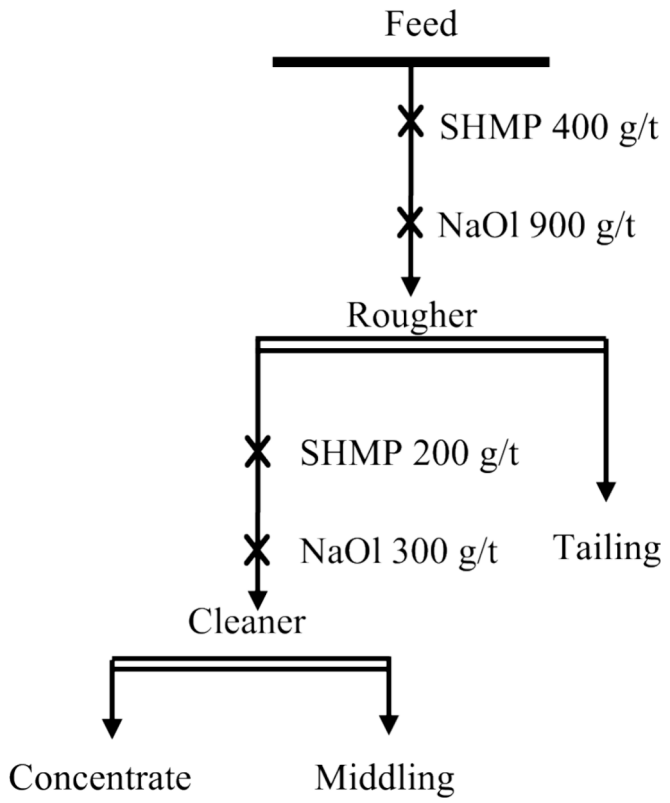

Fig. 11. The flow sheet of laboratory multiple stage flotation by adding a cleaner stage.

Table 7
Flotation results of S5_15kg with multiple stage flotation by adding a cleaner stage, in %.

Part of the sample	Flotation yield, %	Li_2O content, wt %	Li recovery, %	CaO content, wt %	Ca recovery, %
Concentrate	21.60	10.94	30.45	15.11	14.20
Middling	8.72	8.52	9.59	21.41	8.13
Tailing	69.68	6.67	59.96	25.61	77.67
Feed	100.00	7.75	100.00	22.97	100.00

obtained through mineralogical analysis. In flotation research, the highest lithium recovery reached 92.5 %. With the addition of SHMP, the up-floating of the gangue mineral gehlenite could be well inhibited, improving the grade of lithium in the flotation concentrate up to 6.7 wt % (equivalent to 14.4 wt% Li_2O), at which point the lithium recovery drops to 32.8 %.

In NaOl solution, Zeta potential measurements indicated that SHMP is more easily adsorbed on the surface of gehlenite than γ-lithium aluminate. After treatment with NaOl solution, powder contact angle measurements clearly showed that as the concentration of SHMP increased, the powder contact angles of both gehlenite and γ-lithium aluminate decreased. However, greater decrease in gehlenite was observed yielding a selective flotation process.

By designing the EnAM slag and incorporating a flotation process, the silicon content in the feed composition can be reduced before leaching, thereby lowering the silicon content in the leachate, and thus reducing the possibility of silica gel formation.

CRediT authorship contribution statement

Hao Qiu: Writing – review & editing, Writing – original draft, Methodology, Investigation, Data curation, Conceptualization. **Haojie Li:** Writing – review & editing, Software, Methodology, Data curation. **Michael Fischlschweiger:** Writing – review & editing, Methodology, Conceptualization. **Marko Ranneberg:** Writing – review & editing, Methodology, Investigation. **Torsten Graupner:** Writing – review & editing, Investigation. **Hugo Lucas:** Writing – review & editing, Investigation. **Christin Stallmeister:** Writing – review & editing, Investigation. **Bernd Friedrich:** Writing – review & editing, Resources. **Bengi Yagmurlu:** Writing – review & editing, Supervision. **Daniel Goldmann:** Writing – review & editing, Supervision, Resources, Conceptualization.

Table 8
The powder contact angle of γ-lithium aluminate and gehlenite in absence and presence of NaOl and SHMP.

Sample	Powder Contact angle (washburn)	Sample	Powder Contact angle (washburn)
γ-$LiAlO_2$	26°	Gehlenite	58°
γ-$LiAlO_2$ + NaOl 10^{-5} M	88°	Gehlenite + NaOl 10^{-5} M	71°
γ-$LiAlO_2$ + NaOl 10^{-5} M + SHMP 10^{-6} M	90°	Gehlenite + NaOl 10^{-5} M + SHMP 10^{-6} M	47°
γ-$LiAlO_2$ + NaOl 10^{-5} M+SHMP 10^{-5} M	72°	Gehlenite + NaOl 10^{-5} M+SHMP 10^{-5} M	11°
γ-$LiAlO_2$ + NaOl 10^{-5} M+SHMP 10^{-4} M	67°	Gehlenite + NaOl 10^{-5} M+SHMP 10^{-4} M	0°

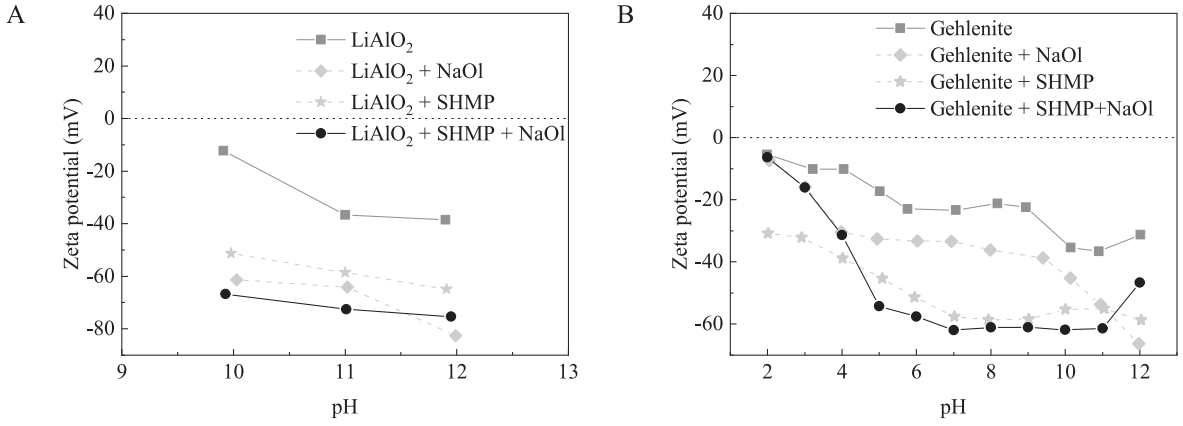

Fig. 12. A. Zeta potential of γ-lithium aluminate as a function of pH in absence and presence of NaOl and SHMP; B. Zeta potential of gehlenite as a function of pH in absence and presence of NaOl and SHMP.

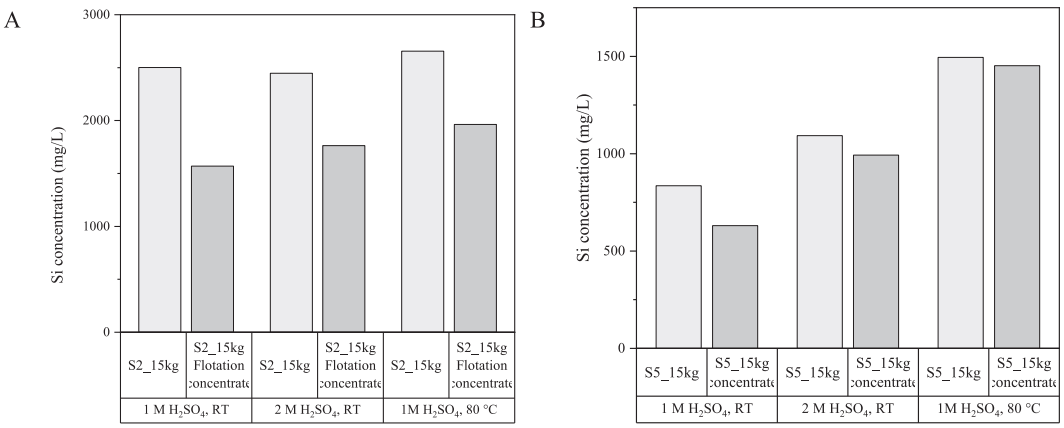

Fig. 13. A. Si concentration of leachate from slag S2_15kg and Si concentration of leachate from concentrate obtained from flotation. B. Si concentration of leachate from slag S5_15kg and Si concentration of leachate from concentrate obtained from flotation.

Declaration of competing interest

The authors declare that they have no known competing financial interests or personal relationships that could have appeared to influence the work reported in this paper.

Data availability

Data will be made available on request.

Acknowledgement

The authors acknowledge the financial support of the German Federal Ministry of Education and Research (BMBF) within the cluster project, “greenBatt PyroLith” (Reference number: 03XP0336A, 03XP0336B and 03XP0336C). We thank Petra Sommer, Heike Grosse for the elemental analysis. We acknowledge Dr. Volker Vogt, Prof. Yihe Wei and Gui Zhang for the insightful discussion.

Appendix A. Supplementary data

Supplementary data to this article can be found online at https://doi.org/10.1016/j.mineng.2024.108918.

References

Alghunaim, A., Kirdponpattara, S., Newby, B.Z., 2016. Techniques for determining contact angle and wettability of powders. Powder Technol. 287, 201–215.
Alvear, F., Gerardo, R.F., Nikolic, S., 2016. ISASMELT™ for Recycling of Valuable Elements Contributing to a More Sustainable Society. In: Kvithyld, A., Meskers, C., Kirchain, R., Krumdick, G., Mishra, B., Reuter, M., Wang, C., Schlesinger, M., Gaustad, G., Lados, D., Spangenberger, J. (Eds.), REWAS 2013: Enabling Materials Resource Sustainability. Springer International Publishing, Cham, pp. 100–109.
Bale, C.W., Bélisle, E., Chartrand, P., Decterov, S.A., Eriksson, G., Gheribi, A.E., Hack, K., Jung, I.-H., Kang, Y.-B., Melançon, J., Pelton, A.D., Petersen, S., Robelin, C., Sangster, J., Spencer, P., van Ende, M.-A., 2016. Reprint of: FactSage thermochemical software and databases, 2010–2016. Calphad 55, 1–19.
Cheret, D., Santén, S. 2005. Battery recycling. European patent No. EP1589121 B1.
Davenport, W.G., King, M., Schlesinger, M., Biswas, A.K., 2002. Chapter 21 - Chemical Metallurgy of Copper Recycling. In: Davenport, W.G., King, M., Schlesinger, M., Biswas, A.K. (Eds.), Extractive Metallurgy of Copper, Fourth Edition. Pergamon, Oxford, pp. 355–365.
Davris, P., Stopic, S., Balomenos, E., Panias, D., Paspaliaris, I., Friedrich, B., 2017. Leaching of rare earth elements from eudialyte concentrate by suppressing silica gel formation. Miner. Eng. 108, 115–122.
Doebelin, N., Kleeberg, R., 2015. Profex: a graphical user interface for the Rietveld refinement program BGMN. J. Appl. Cryst. 48, 1573–1580.
Drzymała, J., Swatek, A., 2007. Mineral processing: foundations of theory and practice of minerallurgy. Oficyna Wydawnicza PWr.
Elwert, T., Goldmann, D., Schirmer, T., Strauss, K., 2012. Phase composition of high lithium slags from the recycling of lithium ion batteries. Wold of Metallurgy - ERZMETALL 65, 163–171.
Elwert, T., Goldmann, D.-I.-D., Schirmer, T., Strauß, K., 2014. Affinity of rare earth elements to silico-phosphate phases in the system Al2O3-CaO-MgO-P2O5-SiO2. Chem. Ing. Tech. 86, 840–847.
Famery, R., Queyroux, F., Gilles, J.-C., Herpin, P., 1979. Etude structurale de la forme ordonnée de LiAl5O8. J. Solid State Chem. 30, 257–263.
Feng, Q., Wen, S., Zhao, W., Chen, Y., 2018. Effect of calcium ions on adsorption of sodium oleate onto cassiterite and quartz surfaces and implications for their flotation separation. Sep. Purif. Technol. 200, 300–306.
Flores, A., Gerardo, R.F., Nikolic, S., Mackey, P.J., 2014. ISASMELT™ for the recycling of E-scrap and copper in the U.S. case study example of a new compact recycling plant. JOM 66, 823–832.
Friedrich, B., Kalisch, M., Friedmann, D., Degel, R., Kaußen, F., Böhlke, J., 2018. The Submerged Arc Furnace (SAF): state-of-the-art metal recovery from nonferrous slags. J. Sustain. Metall. 4, 77–94.
Garrett, D.E., 2004. handbook of lithium and natural calcium chloride. Elsevier Science.
Georgi-Maschler, T., Friedrich, B., Weyhe, R., Heegn, H., Rutz, M., 2012. Development of a recycling process for Li-ion batteries. J. Power Sources 207, 173–182.
Haas, A., Goldmann, D., Schirmer, T., 2018. Challenges and research needs in flotation of synthetic metal phase. GDMB Verlag GmbH, Clausthal-Zellerfeld, Germany.
Fathi Habashi (Ed.), 1997. Handbook of extractive metallurgy. Primary metals, secondary metals, light metals. Wiley-VCH Verlag GmbH & Co. KGaA.
Klimko, J., Oráč, D., Miškufová, A., Vonderstein, C., Dertmann, C., Sommerfeld, M., Friedrich, B., Havlík, T., 2020. A combined pyro- and hydrometallurgical approach to recycle pyrolyzed lithium-ion battery black mass part 2: lithium recovery from li enriched slag—thermodynamic study, kinetic study, and dry digestion. Metals 10, 1558.
Krüger, J., 1999. Metalle–Speisen–Steine–Schlacken; grundlegende Eigenschaften und Reaktionen. In: Schlacken in der Metallurgie. Proceedings of the 35th Metallurgical Seminar of the GDMB-Fachausschuss für Metallurgische Aus- und Weiterbildung, Aachen, Germany, 83, 9–38. Clausthal-Zellerfeld: GDMB-Verlage GmbH.
Lager, G.A., Meagher, E.P., 1978. High-temperature structural study of six olivines. Am. Mineral. 63, 365–377.
Li, H., Qiu, H., Schirmer, T., Goldmann, D., Fischlschweiger, M., 2022. Tailoring lithium aluminate phases based on thermodynamics for an increased recycling efficiency of Li-ion batteries. ACS EST Eng. 65, 13.
Lucas, H.I., Maier, J., Friedrich, B. (Eds.), 2020. The Use of Submerged Arc Furnace (SAF) as a Robust Technology for Upcycling Waste into Standard Mineral Products for Construction Industry. Thomé-Kozmiensky Verlag GmbH, Neuruppin.
Lukas, H.L., Fries, S.G., Sundman, B., 2007. Computational thermodynamics. Fries, Bo Sundman. Cambridge University Press, Cambridge, The CALPHAD method / Hans Lukas, Suzana G.
Ma, Y., Stopic, S., Friedrich, B., 2019. Hydrometallurgical treatment of an eudialyte concentrate for preparation of rare earth carbonate. Johnson Matthey Technol. Rev. 63, 2–13.
Marezio, M., 1965. The crystal structure and anomalous dispersion of γ-LiAlO2. Acta Crystallogr. 19, 396–400.
Marincea, S., Dumitras, D.-G., Ghinet, C., Fransolet, A.-M., Hatert, F., Rondeaux, M., 2011. Gehlenite from three occurrences of high-temperature skarns, romania: new mineralogical data. Can. Mineral. 49, 1001–1014.
Meshram, P., Pandey, B.D., Mankhand, T.R., 2014. Extraction of lithium from primary and secondary sources by pre-treatment, leaching and separation: a comprehensive review. Hydrometall. 150, 192–208.
Mingyu, W.A.N.G., Liaosha, L.I., Li, Z.H.A.N.G., Linnan, Z.H.A.N.G., Ganfeng, T.U., Zhitong, S.U.I., 2006. Effect of oxidization on enrichment behavior of TiO2 in titanium-bearing slag. Rare Met. 25, 106–110.
Müller, T., Friedrich, B., 2006. Development of a recycling process for nickel-metal hydride batteries. J. Power Sources 158, 1498–1509.
Pillars, W.W., Peacor, D.R., 1973. The crystal structure of beta eucryptite as a function of temperature1. Am. Mineral. 58, 681–690.

Politaev, V.V., Petrenko, A.A., Nalbandyan, V.B., Medvedev, B.S., Shvetsova, E.S., 2007. Crystal structure, phase relations and electrochemical properties of monoclinic Li2MnSiO4. J. Solid State Chem. 180, 1045–1050.

Qiu, H., Kersebaum, J., Wollmann, A., Feuge, N., Haas, A., Goldmann, D., Wilhelm, R., 2021. Improvement of the froth flotation of LiAlO2 and melilite solid solution via pre-functionalization. Sci. Rep. 11, 20443.

Qiu, H., Degenhardt, C., Feuge, N., Goldmann, D., Wilhelm, R., 2022. Influencing the froth flotation of LiAlO2 and melilite solid solution with ionic liquids. RSC Adv. 12, 29562–29568.

Ranneberg, M., Lucas, H., Li, H., Graupner, T., Fischlschweiger, M., Friedrich, B. 2023 Evaluation of Li and Mn influence on Al-Ca-Si-O slag system regarding pyrometallurgical LIB treatment. In Proceedings of the 8th International Slag Valorisation Symposium, Mechelen, Belgium; 205-209.

Ren, S., Guo, F., Zhou, J., Yang, J., Yao, L., Kong, M., 2017. Effect of compositions and additives content on crystallization behavior of Ti-rich phase from Ti-bearing blast furnace slag. Metall. Res. Technol. 114, 415.

Ren, G., Xiao, S., Xie, M., Pan, B., Chen, J., Wang, F., Xia, X., 2017. Recovery of valuable metals from spent lithium-ion batteries by smelting reduction process based on FeO–SiO2–Al2O3 slag system. Trans. Nonferrous Met. Soc. Chin. 27, 450–456.

Saunders, N., Miodownik, A.P., 1998. CALPHAD (calculation of phase diagrams): a comprehensive guide. Elsevier.

Schirmer, T., Qiu, H., Li, H., Goldmann, D., Fischlschweiger, M., 2020. Li-distribution in compounds of the Li2O-MgO-Al2O3-SiO2-CaO system—a first survey. Metals 10, 1633.

Schirmer, T., Qiu, H., Goldmann, D., Stallmeister, C., Friedrich, B., 2022. Influence of P and Ti on phase formation at solidification of synthetic slag containing Li, Zr, La, and Ta. Minerals 12, 310.

Sommerfeld, M., Vonderstein, C., Dertmann, C., Klimko, J., Oráč, D., Miškufová, A., Havlík, T., Friedrich, B., 2020. A combined pyro- and hydrometallurgical approach to recycle pyrolyzed lithium-ion battery black mass part 1: production of lithium concentrates in an electric arc furnace. Metals 10, 1069.

Tang, Kai, Ciftja, Arjan, Eijk, Casper van der, Wilson, Shawn, Tranell, Gabriella, 2013. Recycling of the rare earth oxides from spent rechargeable batteries using waste metallurgical slags. J Min & Metal B Metallurgy 49.

Tian, M., Liu, R., Gao, Z., Chen, P., Han, H., Wang, L., Zhang, C., Sun, W., Hu, Y., 2018. Activation mechanism of Fe (III) ions in cassiterite flotation with benzohydroxamic acid collector. Miner. Eng. 119, 31–37.

Vest, M., Zervos, J., Weyhe, R., Friedrich, B., 2010. Slag design for lithium recovery from spent batteries. Int. Work. Met. Interact. 9, 93.

Vignes, A., 2010. Extractive Metallurgy 1. Basic Thermodynamics and Kinetics, Wiley, London.

Voßenkaul, D., Birich, A., Müller, N., Stoltz, N., Friedrich, B., 2017. Hydrometallurgical processing of eudialyte bearing concentrates to recover rare earth elements via low-temperature dry digestion to prevent the silica gel formation. J. Sustain. Metall. 3, 79–89.

Wang, M., Zhang, L., Zhang, L., SUI, Z., TU, G., 2006. Selective enrichment of TiO2 and precipitation behavior of perovskite phase in titania bearing slag. Trans. Nonferrous Met. Soc. Chin. 16, 421–425.

Wittkowski, A., Schirmer, T., Qiu, H., Goldmann, D., Fittschen, U.E.A., 2021. Speciation of manganese in a synthetic recycling slag relevant for lithium recycling from lithium-ion batteries. Metals 11, 188.

Zhang, W., Jiakuan Yang, X.W., Yuchen, Hu., Wenhao, Yu., Wang, J., Dong, J., Li, M., Liang, S.a., Jingping, Hu., Vasant Kumar, R., 2016. A critical review on secondary lead recycling technology and its prospect. Renew. Sustain. Energy Rev. 61, 108–122.

Zhang, N., Nguyen, A.V., Zhou, C., 2018. A review of the surface features and properties, surfactant adsorption and floatability of four key minerals of diasporic bauxite resources. Adv. Colloid Interface Sci. 254, 56–75.

Zhang, L., Zhang, L.N., Wang, M.Y., Li, G.Q., Sui, Z.T., 2007. Recovery of titanium compounds from molten Ti-bearing blast furnace slag under the dynamic oxidation condition. Miner. Eng. 20, 684–693.

Zhang, L., Zhang, W., Zhang, J., Li, G., 2016. Effects of additives on the phase transformation, occurrence state, and the interface of the Ti component in Ti-bearing blast furnace slag. Int. J. Miner. Metall. Mater. 23, 1029–1040.